Indian Journal of Engineering & Materials Sciences
Vol. 30, August 2023, pp. 523-529
DOI: 10.56042/ijems.v30i4. 642

Assessing the Flexural Characteristics of Geofoam using Digital Image Correlation Technique

Parvathi Geetha Sreekantan[a*], Gunturi Venkata Ramana[b], Pawan Singh Nohawar[a]

[a]Geotechnical Engineering Division, CSIR-Central Road Research Institute, New Delhi 110 025, India

[b]Department of Civil Engineering, Indian Institute of Technology Delhi, Hauz Khas, New Delhi 110 016, India

Received: 17 April 2023; Accepted: 16 May 2023

Geofoam is a popular lightweight fill material block used for the construction of road embankments over soft subsoils. The uneven load distribution and excessive settlement over such embankments can lead to differential stress distribution, leading to the bending of thin geofoam blocks. The assessment of geofoam's ability to withstand bending stresses is commonly conducted by evaluating its flexural strength, which also serves as an indicator of its bond strength resistance. In the present study, flexural characteristics of geofoams of varying densities ranging from 15 kg/m^3 to 30 kg/m^3 are assessed experimentally. Subsequently, a statistical assessment is conducted to analyse the variations in flexural strength and modulus and their potential relationship with geofoam density. A non-contact full-field strain measurement during the test is conducted using 2D-digital image correlation (DIC). This facilitated the evaluation of strain distribution within the geofoam during the testing. The observed DIC strains at the outer fibre matched precisely with the physically measured strain, validating the analysis method. It is observed that irrespective of the geofoam density; the EPS cell collapse occurred at a constant true strain value, i.e., 17%. Furthermore, it is also noted that more than 55% of the sample area experiences tensile strain during failure, whereas 45% is subjected to compressive strain. It is also determined that the ratio of the area under compression to tension at failure exhibited an increase in correlation with the density of the geofoam.

Keywords: Bending, Digital image correlation, Expanded polystyrene (EPS), Modulus, True strain

1 Introduction

Geofoams are a type of rigid cellular foam block that found application in diverse construction applications. Due to their significantly lower density compared to soil, as indicated by the ASTM D6817 standard[1], these foams are frequently employed as a lightweight fill material. Since its first application by the Norwegian Public Roads Administration for preventing excessive settlement in 1972[2], geofoams were popularly used for the construction of road embankments resting over soft soil[3–6]. Flexural strength is a crucial parameter for evaluating the suitability of a material in such applications, in addition to compressive strength and elastic modulus[7].

Flexural strength is generally alluded to as the 'quality' of EPS Geofoam[8], since it reflects on the bond strength of the moulded block. Compressive collapse occurs when the cell faces buckle and collapse, whereas, in flexure, the fracture occurs through the beads, or along the bead boundaries[9]. Thus, the flexure test is routinely used for quality checks of the blocks in the geofoam manufacturing units. In general, cellular foams exhibit good flexural strength, which makes them a potential material for pavement applications. Some researchers[10] have observed the bending of the geofoam subgrade as a result of unequal load distribution, particularly at low stress levels. The characteristics of the geofoam subgrade are also critical for the long-term performance of heavy-loading applications such as airfield pavements[11].

Flexural characteristics of geofoam are reported by a few researchers[12–14]. However, none of these studies have reported the flexural behaviour of geofoam using full-field analysis. The recent advancements in digital imaging combined with powerful image processing tools have enabled the development of effective methods for the mechanical characterisation of materials. Full-field strain measurement, in conjunction with physical measurement, facilitates strain evaluation over a wide range of time and area. The digital image correlation (DIC) method has been employed by numerous researchers in previous studies to assess crack propagation and strain distribution in concrete and rocks[15–18]. Nevertheless, there is currently no existing report on the utilisation

*Corresponding author (E-mail: parvathi.crri@nic.in)

of this method for the analysis of the flexural properties of EPS foam. In this study, a comprehensive evaluation of the flexural behaviour of geofoam is conducted using digital image correlation analysis. Following the validation process, the strain field mapping is done for different densities of geofoam and ranges of strain. Furthermore, a statistical assessment and correlation analysis were conducted to examine the relationship of flexural strength and modulus with geofoam density.

2 Materials and Methods

2.1. Materials

For this study, EPS geofoam blocks manufactured in India by two companies, namely, E-Pack Polymers Pvt. Ltd. and Shree Insupac Ltd., were used. Geofoam blocks designated as 15D, 20D, 25D and 30D having respective nominal densities of 15 kg/m^3, 20 kg/m^3, 25 kg/m^3, and 30 kg/m^3, were collected. The measured apparent density and the compression parameters of various geofoam types are listed in Table 1. Specimens of size 300 mm × 100 mm × 25 mm were cut out from the blocks using a hot wire. The Scanning electron microscope (SEM) image of a 30D geofoam block is shown in Fig. 1. It can be observed that EPS beads, which contain numerous closed cells, were moulded together to form a structural block.

2.2 Flexural Test

Four-point flexural tests were carried out as per ASTM C203[21] in a universal testing machine (UTM) of 5 kN capacity with an accuracy of 0.01 N (Model: Shimadzu AGSJ). The inbuilt data-acquisition system records the load-deformation pattern seamlessly at a time interval of 3 ms. Since geofoam is a complex material cellular structure, true strain localisation due to pure bending from a four-point test was necessary instead of a three-point test to understand the full-field flexural behaviour. The strain rate of the outer fibre, R, was estimated from the crosshead motion rate, Z, using equation 1. The rate of crosshead motion was determined as 4 mm/min to maintain a strain rate of outer fibre equal to 0.01. The maximum outer fibre stress, S and strain, ε, were estimated using equations 2 and 3, respectively. The flexural elastic modulus, E_f, was estimated using equation 4. The notations used for the equations are illustrated in Fig. 2. Repeatability was verified through five samples of each nominal density.

$$R = \frac{ZL^2}{6d} \quad \ldots (1)$$

$$S = \frac{3PL}{4bd^2} \quad \ldots (2)$$

$$\varepsilon = \frac{6Fd}{L^2} \quad \ldots (3)$$

$$E_f = \frac{5PL^3}{384\,I\,D} \quad \ldots (4)$$

where L, b and d represent the length, breadth and depth of the sample respectively; P and I indicate the

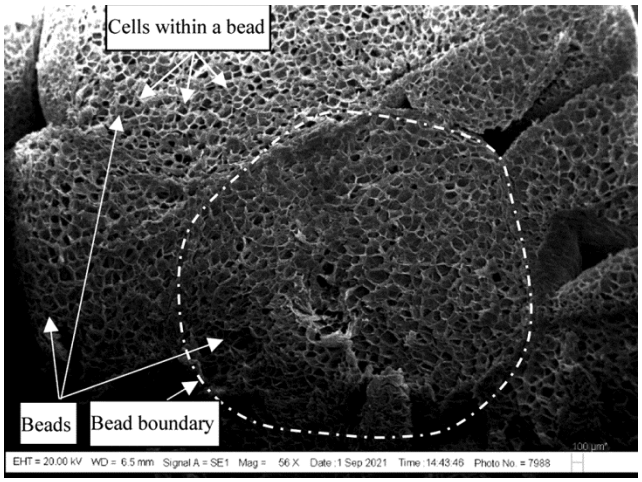

Fig. 1 — SEM image of geofoam block

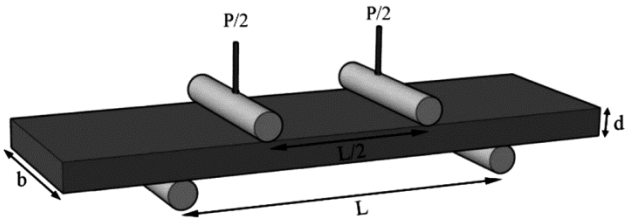

Fig. 2 — Schematic diagram of the flexural test setup

Table 1 — Properties of the geofoam

Property		Test Method	Geofoam Type			
			15D	20D	25D	30D
Apparent Density, (kg/m^3)		ASTM D1622[19]	16.20-16.45	21.54-22.14	25.75-26.00	28.01-28.6
Avg. Density, γ (kg/m^3)			16.32	21.84	25.87	28.30
Compressive resistance (kPa) at strain	1% (σ_1)	ASTM D1621[20]	27	29	44	66
	Yield (σ_y)		72	105	126	167
	10% (σ_{10})		87	119	141	198
Elastic Modulus, E_i (MPa)			2.73	2.93	4.45	6.63

load and the corresponding moment of inertia respectively; D indicates the corrected deflection at the centre of the sample, which is estimated as $\varepsilon L^2/4.363d$; ε and F indicate the strain and deflection at the load fixture position at failure respectively.

2.3 Digital image correlation (DIC)

Digital image correlation is a non-contact method of measuring the deformation of solid objects, facilitating the observation of complex material behaviour during mechanical testing. For DIC, the object is first applied with a random speckle pattern on the surface, which is later used for generating grey values based on the speckle distribution for each pixel of the object image. The region of interest is then divided into numerous virtual grids, named subsets, each of which contains a set of pixels. A search algorithm is used to look for the subset with the same pixels and grey value for identifying the same area after deformation. The displacement of each subset, Q, is measured with respect to the reference image by tracking the centre point of each subset, as shown in Fig. 3. Thus, the in-plane horizontal (*du*) and vertical displacements (*dv*) of subset Q can be calculated. Correlation functions[22] are used for this tracking. Strain fields are later derived by differentiating the displacement of these subsets.

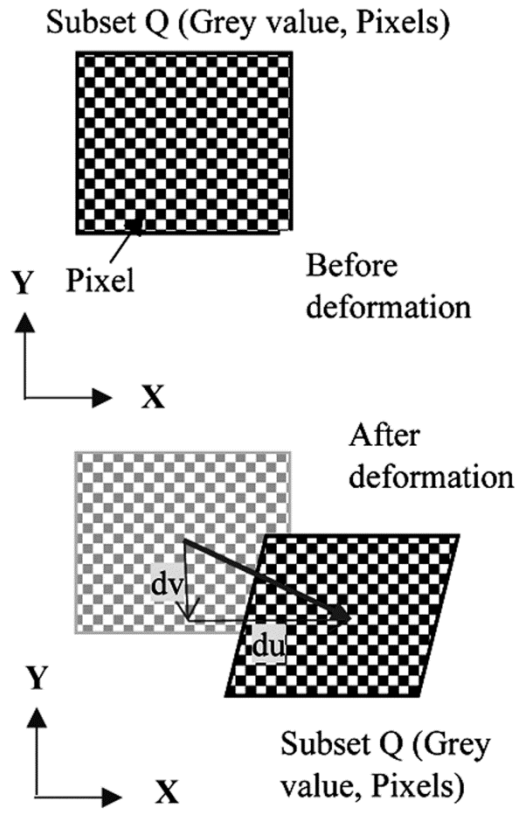

Fig. 3 — Deformation measurement principle of 2D-DIC.

For the present study, a 2D digital image correlation (DIC) system consists of one digital camera, two high-brightness LED illumination lights and a computer with image-capturing software (Fig. 4) was employed. The data analysis of the captured images was carried out using GOM correlate software developed by M/s. GOM GmbH, Germany. The digital camera had a resolution of 24 megapixels and a lens with a focal length of 50 mm. The image was automatically captured at a frequency of 2 s with the help of image-capturing software. The side area of 300 mm width and 25 mm height was considered as the region of interest. The region of interest within the sample for DIC analysis was sprayed with black colour to create a speckle pattern. The speckle pattern's quality was critical for analysis, as low-quality speckles failed to create the subsets with sufficiently defined pixels, leading to analysis errors. Thus, the quality of the speckle pattern was checked prior to the testing. GOM correlate facilitated such a check, unlike other free Matlab algorithms like NCORR and DICe[23]. Comparing the image size and sample size, the actual length of each pixel was calculated to be 0.09 mm/pixel. The subset and spacing used for the analysis were 17 and 18 pixels, respectively. Therefore, a subset size of 1.5 mm, falling within the mesoscale range, was selected for the analysis.

3 Results And Discussion

3.1 General response

Flexural stress, strain and modulus were calculated for each sample. The estimated stress–strain response indicated good repeatability, as shown in Fig. 5. The results also indicated a brittle type of failure. As the

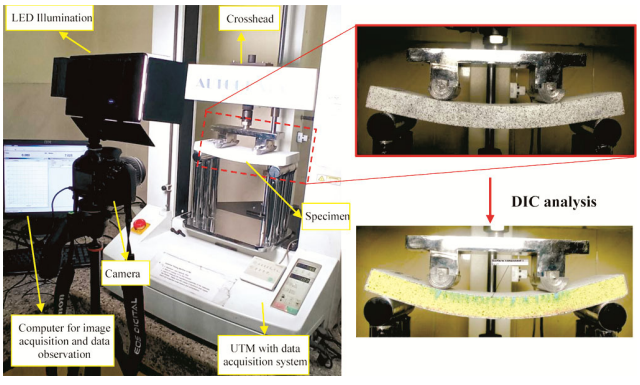

Fig. 4 — 2D DIC set-up for flexural test and image processing sequence of specimen.

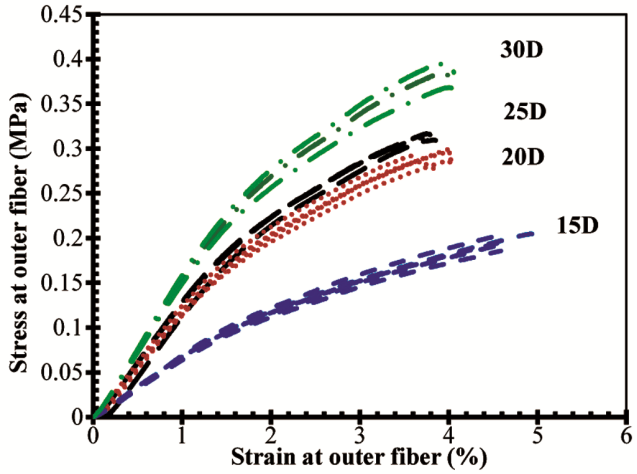

Fig. 5 — Flexural test results.

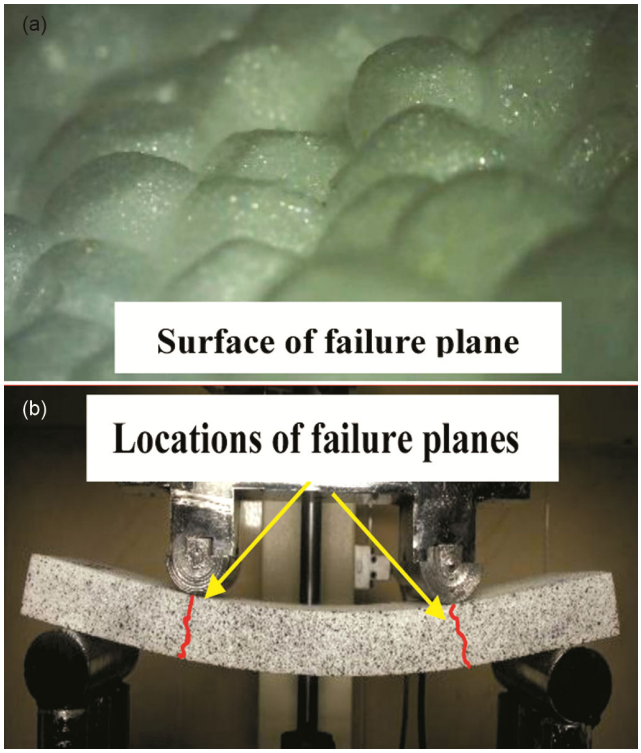

Fig. 6 (a) — Microscopic image of the surface of the failure plane, and (b) location of failure plane.

density increased from 15 kg/m^3 to 30 kg/m^3, failure strain at the outer fibre decreased from 4.5% to 3.7%.

The failure plane was located beneath the loading point, i.e., at L/4 from the specimen edge, as indicated in Fig. 6(a). The microscopic image of the failure plane, as depicted in Fig. 6(b), revealed that the failure plane consistently traversed the bead joints. Consequently, there was no observed occurrence of bead breakage along the plane of

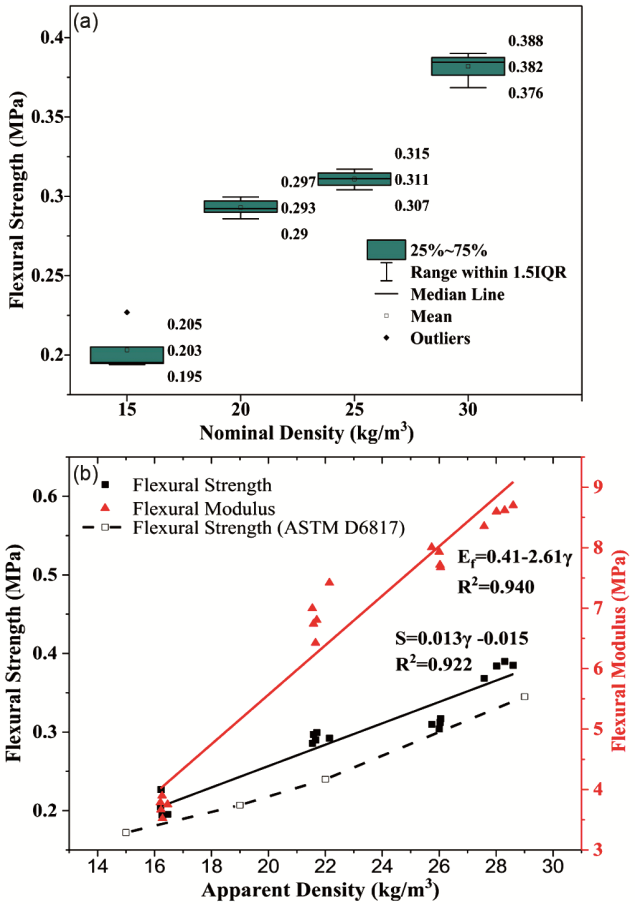

Fig. 7 — Variation of flexural strength with (a) Normal density, & (b) Apparent density.

failure. Therefore, it can be affirmed that the flexural test serves as a reliable indicator of the bond strength of EPS beads.

Fig. 7(a) illustrates the variability of flexural strength data across various grades of geofoam, as represented by box plots. The boxes exhibit a nearly consistent thickness, suggesting a consistent variation in flexural strength across all the nominal densities under consideration. The variation of flexural strength and flexural modulus with respect to apparent density compared to the minimum requirement as per the standard is shown in Fig. 7(b). Flexural modulus followed a linearly increasing trend with density having good convergence (R^2 > 0.9). The empirical correlations of flexural strength and flexural modulus with apparent density are shown in equations 5 and 6, respectively. It can be inferred that all the samples passed the minimum requirement specified in the standard. This indicated a possibility of the negligible effect of other external factors on the flexural behaviour of EPS geofoam.

$$S = 0.41 - 2.61\gamma \quad \ldots (5)$$

$$E_f = 0.013\gamma - 0.015 \quad \ldots (6)$$

where S and E_f are the flexural strength and modulus, respectively, in MPa; γ is the apparent density. in kg/m^3.

3.2. Validation of DIC

The validation of DIC was conventionally conducted by comparing the strains obtained through DIC analysis with the axial strain calculated from the displacement measured by the UTM. In the current scenario, the nominal strain at the outer fibre, determined through physical measurement of crosshead motion, was compared with the average strain obtained through DIC measurement. Figure 8 shows such a comparison with varying time. A complete concurrence between the DIC strain and nominal strain was observed across all types of geofoam.

3.3. Full-field analysis

The strain field image of the entire block face for translational and the major principal strains is shown in Fig. 9. When the nominal strain was 1%, the specimen underwent uniform major principal strain distribution. The translational strain map (strain along X direction) indicated that the upper portion of the mid-half-length of the specimen underwent compression while the lower half tension. The values of maximum compressive and tensile strains within the block were approximately equal.

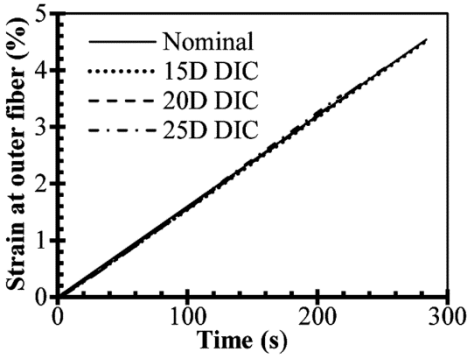

Fig. 8 — Variation of DIC strain to nominal strain.

The strains were maximum at the mid-half-length of the specimen, whereas the end quarters had a uniform strain distribution. In the mid-half-length, the compressive strain field was larger compared to the tensile field. The maximum tensile strains occurred at the mid-base of the specimen. Based on the analysis of the translational strain field, it was possible to deduce that the upper section of the specimen exhibits localised vertical strain bands as a result of compression. The strain bands observed in all types of geofoams are confined to a depth of one-third of the specimen, suggesting that the neutral axis was located at a depth of 0.3d.

The initiation of fracture took place at the location characterised by the highest magnitude of the major principal strain, situated below the applied load. The observed location of the failure plane in the specimen aligns precisely with this statement. This is also in confirmation with the similar studies on fracture analysis on non-homogenous materials[18,24]. Furthermore, it is worth noting that the magnitude of major principal strain at failure for all geofoam types was identical and occurred at the outer fibre of the specimen.

The translational strain field at failure for different geofoams is shown in Fig. 10. It can be deduced that immediately prior to the failure event, certain analysis

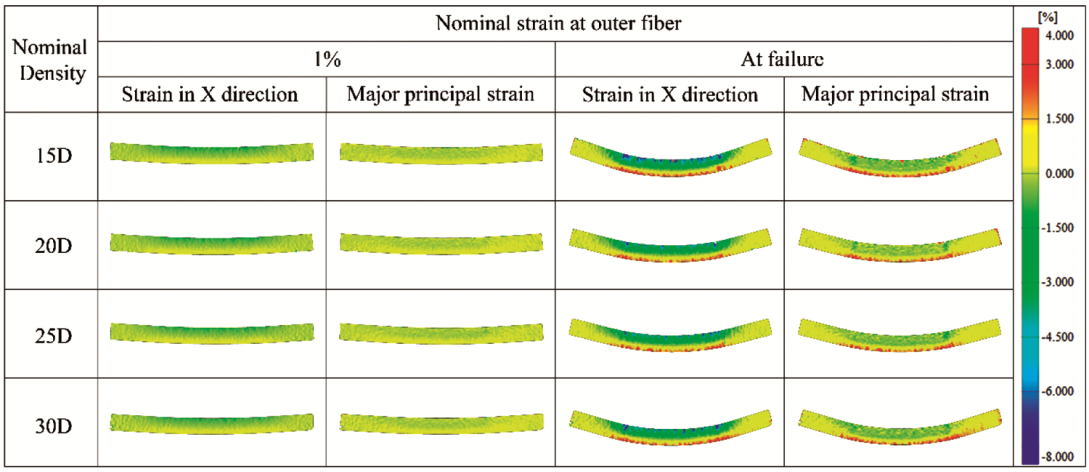

Fig. 9 — Strain field maps.

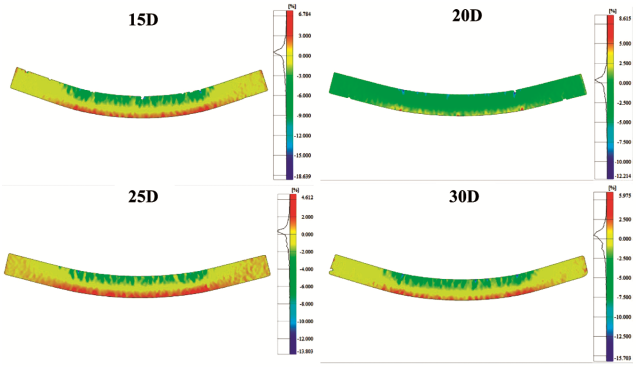

Fig. 10 — Translational strain field maps at failure.

Table 2 — Compression to tensile strain distribution at bending failure

Geofoam grade	A_c: A_t*
15D	1: 1.30
20D	1: 1.30
25D	1: 1.23
30D	1: 1.15

*A_c – Area under compression; A_t – Area under tension

points became merged within the compression zone, as the actual compressive strain surpassed 17%, thereby signifying the collapse of the cell. The histogram showed that the variation of these maximum translational strain with respect to geofoam grade is negligible. Author's previously published study also reported a cell collapse in geofoam during uniaxial compression[25].

The frequency distribution histogram depicted in Fig. 10 was subjected to analysis using Image J software in order to quantify the compression and tensile zones. The analysis reveals that a majority of the sample area, specifically over 55%, experiences tensile stress during failure, whereas approximately 45% was subjected to compressive stress. Table 2 presents the ratio between the sample area under compression and tension at the point of failure for various geofoam grades. As the density of the specimen increases, there is an observed increase in this ratio. Nevertheless, the magnitudes of maximum and minimum strains remained consistent across various grades of geofoam. This finding suggests that there was a more efficient distribution of load in a specimen with high density as compared to a specimen with low density. It can also be recommended that the maximum differential strain within a geofoam block should be limited to 1%. This will ensure that the compressive strain in the top portion of the block is limited to 1%, keeping the specimen in the elastic zone.

4 Conclusion

In this study, the flexural behaviour of EPS geofoams with nominal densities varying from 15 kg/m^3 to 30 kg/m^3 is investigated with the aid of the digital image correlation method. The variation of flexural response with varying apparent density and strain is captured in this study using strain field mapping. The following important conclusions are arrived at, from the study.

- Flexural test indicates a brittle type of failure and the failure plane passed through the EPS bead joints. Failure strain at outer fibre decreases from 4.5 % to 3.7 % as density increases from 15D to 30D.
- The distribution of strains within the block is uniform in the elastic response range, whereas it is heterogeneous with the formation of vertical failure bands in the plastic response range.
- Crack initiation point can be well demonstrated from the major principal strain field obtained from the DIC technique. Cell collapse is observed at a true compressive strain of 17% for all the geofoam grades.
- The maximum and minimum strain values are similar for all the geofoam grades. However, as the density increases, the ratio of specimen area under compression to tension increases, indicating more efficient distribution of load.

Acknowledgement

This work was supported by the National Highways and Infrastructure Development, New Delhi, India (GAP-4658). The approval and support of the Director, Council of Scientific and Industrial Research - Central Road Research Institute (CSIR – CRRI), New Delhi, India 110025, to publish this research paper is also acknowledged. The authors acknowledge the central research facility, IIT Delhi, for the usage of the Scanning electron microscope.

References

1 ASTM D6817, *ASTM International*, (2021)
2 Aabøe R, Bartlett S F, Duškov M, Frydenlund T E, Mandal J N, Negussey D, *et al.* Geofoam Blocks in Civil Engineering Applications. In: Arellano D, Özer AT, Bartlett S F, Vaslestad J, editors. *5th International Conference on Geofoam Blocks in Construction Applications*. (Cham: Springer International Publishing, USA).
3 Puppala A J, Ruttanaporamakul P,. *Geotextiles and Geomembranes,* 47 (2019) 295
4 Özer A T, Akinay E. C *Geosynthetics International* 2022.
5 Abdelrahman G, El Kamash W. *American Society of Civil Engineers,* (2014) 557.

6 Mohajerani A, Ashdown M, Abdihashi L, Nazem M, *Construction and Building Materials*, 157 (2017) 438.
7 ASTM 7180, *ASTM International*, (2021).
8 Wang C. *Characterizing, testing, and modeling the mechanical properties of recycled-content expanded polystyrene-block geofoam*, Ph D thesis, The University of Memphis, 2015.
9 Voiconi T, Linul E, Marşavina L, Sadowski T, Kneć M.. *Solid State Phenomena*, 216 (2014) 116.
10 Huang X, Negussey D.. *Denver, Colorado, United States: American Society of Civil Engineers,* (2007) 1.
11 Barker W, Alexander D. Determining the effective modulus of subgrade reaction for design of rigid airfield pavements having base layers. Technical Report No. ERDC/ GSL-TR-12-20. *US Army Corps of Engineers, Engineer Research and Development Centre* (2012).
12 Beju Y Z, Mandal J N, *Procedia Engineering.* 189 (2017) 239.
13 Solomon A A, Hemalatha G, *Structures*, (2020) 204.
14 Wang C, Arellano D, *American Society of Civil Engineers*, (2014) 3506.
15 Munoz H, Taheri A, Chanda E K, *Rock Mechanics and Rock Engineering*, 49 (2016) 2541.
16 Bu J, Chen X, Hu L, Yang H, Liu S, *International Journal of Concrete Structures and Materials*, 14 (2020).
17 Chai J, Liu Y, Ouyang Y B, Zhang D, Du W, *Advances in Civil Engineering,* 2020 (2020) 11.
18 Mahal M, Blanksvärd T, Täljsten B, Sas G, *Engineering Structures,* 105 (2015) 277.
19 ASTM D1622, *ASTM International*, (2020).
20 ASTM D1621, *ASTM International,* (2016).
21 ASTM C 203, *Indian J Eng Mater Sci*, 20 (2013) 237.
22 Jorge Z, Ronny P, Sotomayor O, *Materials Today: Proceedings*, 49 (2022) 79.
23 Li D, Zhu Q, Zhou Z, Li X, Ranjith P G, *Engineering Fracture Mechanics*, 83 (2017) 109.
24 Sreekantan P G, Vangla P, Ramana G V, *Geosynthetics International*, (2023) 1.